CHAPTER 2

EXPERIMENTAL TECHNIQUES

2. EXPERIMENTAL TECHNIQUES

The present chapter explains the methods used for sample preparation which was by electrodeposition and electron beam (e-beam) sputtering and the various techniques used for analysis of the samples. Following this, all instrumentation used in the analysis process are elaborately discussed as to further show the significance of the results obtained.

2.1 Method of Sample Preparation

The method of sample preparation chosen here are electrodeposition and electron beam sputtering. The objective behind the choice of these two sample preparation techniques is to make an experimental comparison encompassing the following:

- Practicality and ease of deposition
- Cost effectiveness
- Accuracy of ternary compound prepared
- Differences in physical characteristics
- Solar cell performances

The samples produced in this research were thin films of CdTe, CdSe and a combination of the two, $CdTe_XSe_{1-X}$, which were deposited on the following substrates:

- Single Crystal Silicon Wafers - Electrodeposition & Sputtering
- Indium Tin Oxide (ITO) on glass - Electrodeposition & Sputtering
- Glass - Sputtering only

2.2 Electrodeposition

The main technique used in material fabrication here is the electrodeposition method. Emphasis was given to this technique as it is one of the goals of this research to utilise waste silicon wafers from the semiconductor industry for the formation of solar cells using a low temperature and low cost process. Electrodeposition is a well established method that has been known to produce films of electronic and fast ionic conducting materials accurately [44-48]. Basically this method uses two conducting or semiconducting electrodes that function as the anode and cathode which are dipped in an aqueous solution which is the electrolyte. By the passage of current through the system, a chemical decomposition of the electrodes and electrolyte takes place in a phenomena that is identical to electrolysis. The intended material to be fabricated is deposited as a film on the anode or cathode, depending on whether it is an anodic or cathodic deposition, and this is the fundamental principle of the ~~of the~~ electrodeposition process. A photograph of the apparatus used in the electrodeposition process and a schematic drawing of the components is shown in figure 2.1.

Electrodeposition has been a widely researched technique as an attractive option to high temperature physical deposition processes such as sputtering and vacuum evaporation. As it is a low temperature process, it does not need any vacuum apparatus setup and has relatively inexpensive capital outlay for equipment purchases. This tremendously reduces the cost of thin film sample preparation. It is also well favoured over chemical deposition techniques such as spray pyrolysis and CVD due to minimal wastage of materials such as chemicals in its process. In an industrial scenario material costs, equipment costs, time consumption and labour intensiveness are key points of consideration when choices of techniques are evaluated.

The goal of fabricating the thin film materials here is to obtain photovoltaic cells and consequently to study their performance characteristics. For this purpose, there are numerous variable parameters that can be varied that could affect the composition, morphology, adhesiveness and the thickness. They include:-

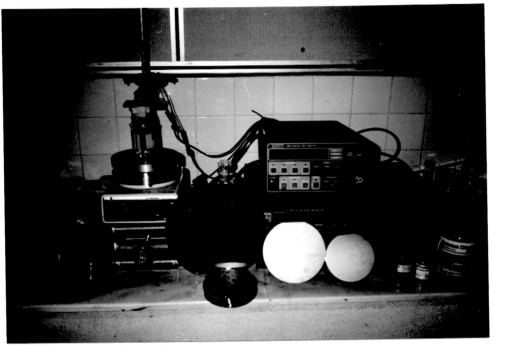

A Photograph of the Apparatus Setup

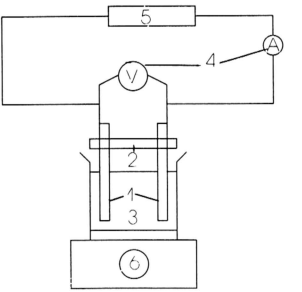

1. Electrodes
2. Insulating Electrode Seperator
3. Electrolyte
4. Multimeters to measure current and voltage
5. SMU-Source Measuring Unit (as power supply)
6. Magnetic stirrer with heater

Figure 2.1 : The components for a basic electrodeposition setup

- Voltage
- Electrolyte concentration
- Deposition time
- Current density
- Temperature

The effect of these parameters were carefully researched in the individual data chapters (chapters 3,4 and 5) prior to the final stages of electrodeposition for solar cell studies.

2.2.1 Voltammetry

The purpose of studies on voltammetry is to investigate the codeposition voltage of two or more ionic species in an electrolyte [49]. It can also be further used to study the effect of current density as a function of applied potential in the electrodeposition process.

For example, for the deposition of CdSe, the voltammetric behaviour of the component electrolytes, $CdSO_4$ and SeO_2, were individually plotted on a voltage versus current plot for specific concentrations. Then the voltammetric curve was plotted for an electrolyte containing both the aqueous solution mentioned above. From this plot the codeposition voltage of the two ionic species of Cd and Se can be clearly determined. A practical application of such a study is described with diagrams in chapter 3.

2.2.2 Cathodic Polarisation

For the electrodeposition of an alloy, each anion species of the electrolyte has to be able to be deposited on the cathode at any given fixed condition of the electrodeposition bath. The common potential can be obtained by studying the increase in deposition current with respect to the potential and consequently plotting this curve for the individual anion species in the electrolytic bath. This analysis can show the cathodic

polarisation behaviour of the electrolyte and the potential required for a 1:1 ratio alloy can be determined.

For example, if the deposition of CdSe in a 1:1 ratio is desired, a study is done on the polarisation behaviour of the electrolyte constituents, namely SeO_2 and $CdSO_4$. Guided by literature on voltammograms [49] and voltage values [50], as well as some experimental investigation, the concentration of SeO_2 was altered to obtain an intersection of these two curves due to ionic exhaustion of selenium ions. A practical example of this approach is shown in chapter 3.

This information, coupled with the information from reported voltammogram assisted in determining the most suitable range of voltage where codeposition of the anions would take place.

2.2.3 Substrate Cleaning

The substrates used for the electrodeposition process have to be cleaned thoroughly to remove all traces of contamination. The method of cleaning silicon wafers need to be put through an additional step, whereby the native oxide layer has to be etched away. This insulating oxide layer could prove to be detrimental for solar cell applications if they are too thick but very thin layers would form a semiconductor-insulator-semiconductor (SIS) junction which is applicable for solar cell purposes. The cleaning of silicon and etching of the oxide layer is shown as a three step process below:

- Boiled in H_2O:H_2O_2:HCl solution with a ratio of 86:11:3
- Immersed in H_2O:H_2O_2:NH4OH with a ratio of 4:1:1
- Immersed in H_2O:HF in a ratio of 10:1

The substrate was rinsed in double distilled water after each step and stored in a dessicator to minimise exposure to moisture.

2.3 Electron Beam Sputtering

The sputtering of the semiconducting thin films was achieved using an Edwards AUTO 306 electron beam sputtering equipment. This apparatus has three main components, namely the vacuum pumping system, vacuum chamber and an electron beam power supply. Figure 2.2 shows the schematic view of the sputtering apparatus.

The vacuum system is necessary as the principle behind this method of sputtering requires electrons from a heated filament to transverse through free space before bombarding and evaporating the target. Without high vacuum, the filament would burn out and the electrons as well as the evaporated target material would not be able to travel far due to collisions with air molecules. The high vacuum is attained by means of an oil diffusion pump backed by a rotary pump. The entire vacuum cycle is controlled by microprocessor controlled solenoid valves.

Figure 2.3 shows a plan view of the vacuum chamber. It comprises of a six position turret source with rotary drive indexing and height adjustment, bell jar, implotion guard, source shutter, substrate holder, electrical heater and a thermocouple. The source of the electron beam is a tungsten filament powered by a 900W electron beam power supply which can supply high tension voltage (HTV 4.5kV ± 10%), high tension current (HTC = 100mA ± 10%), low tension voltage (LTV 6V) and low tension current (LTC, 20A).

Before the deposition cycle, the substrates were cleaned throughly (as prescribed in 2.2.2) and mounted above the target. The source material in granular form and of analar grade, is placed in a carbon hearth and moved into the ready position below the filament. The vacuum chamber bell jar is then replaced and the system is evacuated up to the pressure of 2 x 10^{-5}mbar (in the high vacuum level range). Before the e-beam sputtering was commenced, the filament and source is first degassed with the sample shutter shielding the substrates from heat and contamination from volatile constituents.

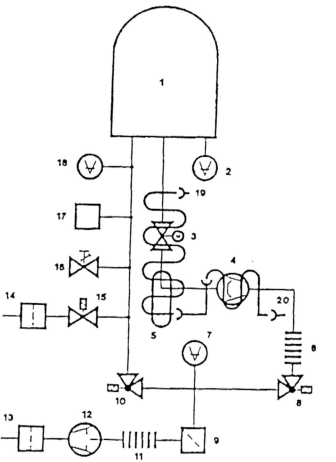

Figure 2.2 : Schematic View of the Sputtering Apparatus

1. Vacuum Chamber
2. Penning Gauge
3. High Vacuum Valve
4. Diffusion Pump
5. Liquid Nitrogen Trap
6. Flexible Coupling
7. Pirani Gauge (Backing)
8. Backing Valve
9. Foreline Trap
10. Roughing Valve
11. Flexible Coupling
12. Rotary Pump
13. Oil Mist Filter
14. Air Admit Filter
15. Air Admit Valve
16. Gas Admit Valve
17. Vacuum Interlock Switch
18. Pirani Gauge (Chamber)
19. Water Inlet
20. Water Outlet

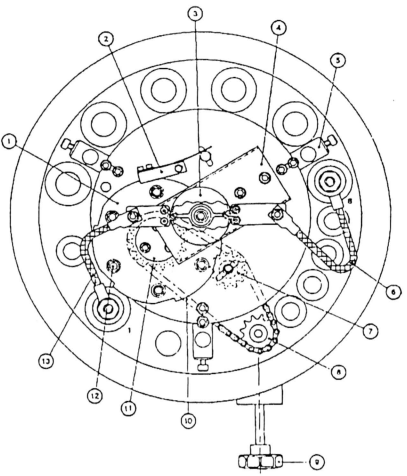

Figure 2.3 : Plan View of the Vacuum Chamber

1. Turret
2. Index Spring
3. Electron Beam Gun
4. Carrier
5. Tripod Mounting Lug
6. Live Braid
7. Tension Sprocket
8. Drive Sprocket
9. Drive Knob
10. Drive Chain
11. Turret Sprocket
12. Turret Source Holder
13. Live Braid

Degassing was achieved by applying low tension (LT) gradually until degassing takes place at about 60% power. The degassing was accompanied by a rise in chamber pressure and the LT was always manipulated to maintain the pressure below 9×10^{-3} mbar. This process was continued until the pressure reaches a steady level before the LT is shut off.

Upon completion of degassing, the system will once again pump down to 2×10^{-5}mbar and will be then ready for commencement of sputtering. The sputtering was achieved by applying high tension voltage (HTV) of 4kV. The low tension current (LTC) was switched on again and gradually increased until an emission current between 50-100mA was achieved. When the source began to evaporate (indicated by a purple glow), the source shutter was opened and the evaporated material was allowed to deposit on the substrate for a period of time depending on the desired film thickness. Upon completion, the source shutter was again closed and the LT and HT were switched off. Even though the substrate was not heated, the rise in temperature due to impinging ions was monitored via the thermocouple and found to be approximately 60°C throughout the process.

To achieve sputtering by this technique, a concentrated beam of high energy electrons was focussed to bombard and consequently evaporate the source material. A heated tungsten filament was used as a thermionic electron source and these electrons were accelerated by using high tension (HT) to impinge on the source at high velosities. The acceleration was due to the filament being at HT and the source at ground potential. The filament was placed cylindrically around the source but out of the path of the evaporation to avoid filament dissolving. The electron beam was pulled down and focussed to the target by a magnetic field. The evaporated source will then traverse through a high vacuum (about 2×10^{-5}mbar) path at their thermal velocities, in a straight line, until they reach the substrate which is placed above the source.

When electron bombardment took place, the beam was directed to the centre to avoid hitting the carbon hearth (source container). The evaporation took an angular lobe

shaped pattern due to the collimating arising from the depression surface. This in effect caused a thickness variation from the centre to the edge of the deposition area, the centre being the thickest. In some systems, the beam is directed in a roster pattern with electromagnetic coils to avoid this effect and the hearth is water cooled to avoid outgassing or alloying with the molten source material.

Some of the problems associated with this technique is outlined below.

• ***Macro-Particle Splitting***

This phenomenon occurs there is a contamination nodule in the source that suddenly bursts due to a vapour pressure which is higher than the source. When the intense energy beam hits this contamination, a sudden pressure burst can knock out a marco particle solid or liquid material typically 0.1 to 1μm in diameter and could land on the depositing film. This problem can be avoided by using a source of high purity.

• ***X-Ray and Positive Ion Generation***

Although generally being a thermal process with vapour atoms leaving the surface with an energy of 0.2eV, sputtering can also cause x-rays to be generated as a consequence of bombarding the source atoms with high energy electrons. The intensities of x-rays are very small and harmless to the operator but could affect the sputtered samples. For example, dielectric material for electronic applications could develop undesired charge-trapping defects or embedded charge due to these x-rays.

Positive ions from the impact of the beam could be accelerated to the substrate because of its negative bias. Since the energy flux is large, it could affect the deposited film structure.

2.4 Material Characterisation

i. The X-ray Diffraction analysis was carried out using a Philips PW1830/40 x-ray Diffractometer with a CuKα radiation (λ = 0.15418nm) to deduce the phase of the material as well as for crystal identification and orientation. Based on the diffractograms, the formation of a new single phased ternary compound was identified.

ii. Micrographs from a Scanning Electron Microscope (Philips XL 40 SEM) were used to help deduce the formation of the deposited material in terms of the surface morphology and uniformity. The materials were mounted on Aluminium stubs with carbon dag, a conducting adhesive, for this purpose.

iii. Quantitative analysis of the material was carried out using Energy Dispersive Analysis of X-rays technique on the EDAX (PV9800) system coupled with the Philips 515 Scanning Electron Microscope. The relative percentages of the elements of interest can be obtained by this method.

iv. Due to the opaque nature of silicon wafers, parellal depositions using identical electrodeposition parameters were done on ITO. Samples deposited by the sputtering process were coated on glass and ITO for the same reasons. The instrument used for this purpose of optical characterisation was the Shimadzu UV-3101PC, for the UV and visible analysis where both the absorption and transmission spectra were recorded.

2.4.1 X-Ray Diffractometry

X-ray crystallography or x-ray powder diffractometry uses single crystals or powder for the identification of compounds by their diffraction patterns [51,52]. The x-ray region of the electromagnetic spectrum (0.1-100 A) is bound by the γ-ray region and the ultraviolet region. The energy of x-rays are usually between 0.1 and 100 keV and is represented by the equation,

$$\mathbf{E} = h\upsilon$$

where h = Planck's constant

υ = frequency

The typical intensity distribution of irradiated x-rays would indicate a broad band of continuous radiation and characteristic discrete wavelengths superimposed on top. Continuous radiation occurs due to the deceleration of the excited electrons due to the interaction of impinging electrons and those of the target element. The characteristic radiation arises from the rearrangement of the orbital electrons of the target element following the ejection of electrons in the excitation process. There are a great number of possibilities for electron transitions when the quantized state of each electron is considered, but in practice, the x-ray spectra has just three selection rules to cover the transitions, being :-

$$\Delta n \geq 1$$

$$\Delta l = 1$$

$$\Delta J = 0 \text{ or } 1$$

where n = group quantum number

l = angular quantum number

J = vector sum of the angular and spin quantum numbers

When an x-ray is incident onto a sample various processes may occur.

1. Absorption : A certain fraction (I/I_O) of the radiation may pass through maintaining the wavelength and the intensity of the transmitted beam is given by

$$\mathbf{I}(\lambda_0) = \mathbf{I_0} \exp - (\mu\rho x)$$

where μ = mass desorption coefficient

x = thickness

ρ = density

2. Photoelectric effect : An intensity $(I - I_0)$ has been lost due to this effect and it will occur at each of the energy levels of the atom.

3. Scatter : This phenomenon occurs when an x-ray photon collides with the electrons of the sample. If an elastic collision occurs, no energy is lost and the scatter is said to be coherent (Rayleigh Scatter) and the scattered radiation will have the same wavelength as the incident radiation. If the collision is inelastic (Compton Scatter), the x-ray photon loses part of its energy and this is called incoherent scattering and the wavelength of the scattered radiation will no longer be equal to the incident radiation.

The total scatter is represented by :

$$\sigma = \underset{\text{coherent}}{(Zf)^2} + \underset{\text{incoherent}}{Z(1 - f^2)}$$

where f = electronic structure factor

A crystal can be defined as a homogenous, ansiotropic body having the natural shape of a polyhedron. In x-ray diffractometry, solids which have a low degree of order are known as glassy materials and may show fluid properties but most solids are crystalline. a crystalline substance has a definite form independent of the crystal size. Basically there are seven crystal types forming unit cells namely:- cubic, tetragonal, orthorhombic, hexagonal, monoclinic, triclinic and rhombohedral, where each type has its own symmetry operation which is unique to itself. The symmetry element can cause diffraction intensity of certain planes to increase due to the multiplicity effect which is the effect due to several planes being in reflecting positions.

To illustrate the diffraction phenomenon, a model of the crystal lattice consisting of sets of parallel planes separated by distance, d, as shown in figure 2.4. The condition for diffraction can be found in two steps:

a. the waves of all atoms lying in a single plane must be in phase
b. the scattering of waves in successive planes must also be in phase

Condition (a) is fulfilled if the incident ray, the diffracted ray and the normal to the reflecting surface all lie in one plane and if the incident angle equals the reflection angle. The condition (b) is illustrated when two parallel rays strike a crystal at angle θ, reinforcements will occur when the difference in the path length of two rays is equal to a whole number of wavelengths. From figure 2.4, we can see that the difference of path length, n = CB + BD, and since CB = BD = X, we say n = 2x. Geometrically $x = d\sin\theta$, hence $n\lambda = 2d\sin\theta$. This is actually Bragg's Law governing the phenomena of diffraction.

The x-ray powder diffractometer consists of three main parts, the x-ray tube as a radiation source, the diffractometer and the detector and counting equipment. The construction of an x-ray tube is shown on figure 2.5. A tungsten filament is heated by passing current to emit electrons and these electrons are accelerated by an anode potential of 30 - 60kV. The conversion of electrons to x-rays is an inefficient process and the heat generated has to be cooled by water and the tube is constructed of copper to ensure good cooling. The filament is in a Wehnelt cylinder which focuses the electron beam. The anode material used is usually copper, which would incidentally emit CuKα radiation.

Figure 2.6 shows a typical geometry of a powder diffractometer, which is known as Bragg-Brentano focusing geometry. This is typified by a diverging beam from a line source F, falling on specimen S, being diffracted and passes through a receiving slit R, into the detector. The distance FA and AR are equal and the divergence is determined by the effective focal size and D which is matched with a scatter slit SS. Lateral divergence is controlled by two sets of parallel plate vertical collimators P and RP.

Figure 2.4 : Conditions for X-Ray Diffraction

1. Atomic Lattice Spacing
2. Incident X-Rays
3. Diffracted X-Rays

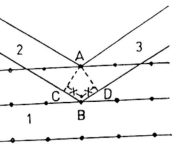

Figure 2.5 : X-Ray Tube Configuration

a. Filament Spiral
b. Filament Leads
c. Wehnelt Cylinder
d. Anode
e. Anode Block
f. Beryllium Window
g. Water Filter Assembly
h. Safety Lead Insert
I. X-Ray Tube Tower
j. β-Filter Assembly

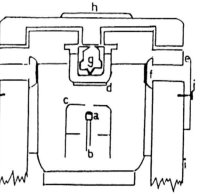

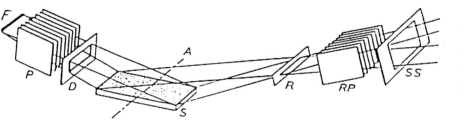

Figure 2.6 : Geometry of a Diffractometer

F. Line Source
R. Receiving Slit
S. Specimen
P&RP. Vertical Collimators
D. Diffraction Slip
SS. Scatter Slip

There are three basic detection systems in a XRD instrument :

1. Proportional Detectors - which is the detector used here and is excellent for application with Cu or softer x-rays.

2. Scintillation Detector - more suitable for Mo radiation rather than Cu. This detector has poorer energy resolution and higher intrinsic background noise.

3. Solid State Detector - this has good energy resolution and low background and suitable for low signal applications. However, it has a low maximum countrate, poor linearity and is not suitable for quantitative analysis

2.4.2 Scanning Electron Microscopy

For the purpose of surface analysis, the Scanning Electron microscope (SEM) technique seemed ideal as a significant amount of information on the microstructure can be obtained [53,54]. From the micrographs obtained, we are able to note :-

1. The uniformity of the deposition surface
2. Structural faults due to surface and internal mechanical stress
3. Surface deformities

The SEM method utilises an electron beam instead of visible light to overcome magnification limitation due to the incident beam wavelength and the performance of optical lenses. Figure 2.7 shows the components of a scanning electron microscope.

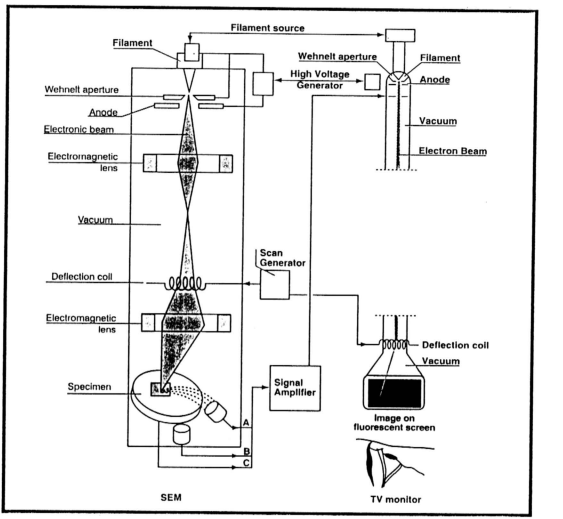

Figure 2.7 : Components of a SEM

A basic SEM consists of four major components being an electron gun, a demagnification unit, a scan unit and a detector system. The electron source is a thermally heated tungsten filament at the top of the microscope column. The electrons are subjected to focusing via the negatively biased wehnelt cylinder and forms the first crossover in the range of 10-30 microns from the filaments. The electrons are then accelerated by applying a highly negative biasing voltage between the anode and cathode in the range of 200eV to 30keV.

Analogous to optical lenses in a light microscope, two electromagnetic lenses are used to demagnify the filament crossover and focus it onto the specimen. There are a set of scanning coils above the final lens to enable the electron beam to be systematically moved over a selected area of the sample in a raster pattern. When the sample is bombarded by an electron beam, various electrons are emitted such as secondary electrons (SE) and backscatter electrons (BSE) as well as the cathodoluminiscence (CL) phenomena. Any one of these emissions can be utilised for the purpose of imaging.

In this circumstance, secondary electrons are detected with a dedicated detector and converted into a voltage signal which in turn varies the brightness of a synchronously operating cathode ray tube (CRT). The SE detector used for specimen imaging contains a biased grid at about +300V which attracts SE and a possible -150V bias which would attract BSE. The electrons are accelerated to about 10keV and hits a scintillator. The generated light is fed through a light guide to a photo-multiplier where the signal is amplified for voltage-brightness modulation.

The scanning coupled with the modulation of signal intensity produces a TV image on the CRT. The magnification is denoted by the ration of the CRT size in comparison to the area of the specimen thus is scanned. The resolution of the micrograph, which is defined by the closest distance between specimen details, is determined by the diameter of the electron beam that can be controlled by varying the field in the condensor lens.

The image produced on the CRT can be captured on a 35mm camera to be reproduced in high clarity. Additional coils in the microscope assist in the alignment of the gun tilt and shift, and stigmator coils counters the effect of astigmatism due to inhomogenous magnetic fields in the lenses.

2.4.3 Energy Dispersive Analysis of X-rays (EDX)

The EDX technique has been proven to be an accurate and rapid technique of obtaining quantitative data of elements in microanalysis [55]. X-rays being photons of electromagnetic radiation are distinguished by their wavelength range of about 0.1 to 100 Angstroms and originate from events occurring in the structure of an atom. The basic principle behind EDX analysis is that characteristic X-rays have energies that can be identified with the element that produced them. These are obtained when an empty spot is obtained within the atom due to an electron removal by ionisation or excitation. This excitation can be obtained by electron beams (as in the case of EDX), charged particles like protons or alpha particles and by photons from other X-rays or γ-rays. The various forms of excitation have different probabilities of creating electron vacancies and these probabilities vary in a complex manner with energy, atomic number, absorption and fluorescence.

The EDX detector is coupled to the SEM as the electron beam in the system, which goes up to a maximum energy of 30keV, is sufficient to generate characteristic X-rays from the specimen. Electrons in an atom have energy levels which are known as K, L, M, N, etc., where the K shell is the most strongly bound to the nucleus. X-rays are emitted when a vacancy in a particular shell is filled by electrons from other shells. If an electron is ejected from the K shell and the vacancy is filled by an electron from an L shell, an x-ray photon called Kα is released. If the electron comes from an M shell, it is referred to as Kβ.

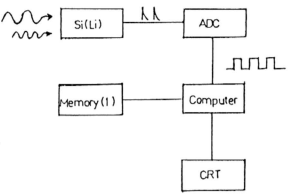

Figure 2.8 : Setup for EDX Detection System

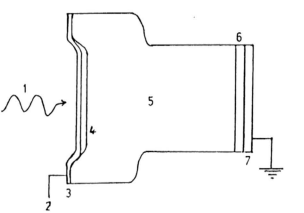

Figure 2.9 : Cross Section of a Detection Crystal

1. Incident X-ray Photons
2. 750V Biasing Voltage
3. Gold Contact
4. Si Dead Layer
5. n-type Si
6. Metal Contact

The nature of the sample determines the energy range of the characteristic x-ray. This characteristic emission is randomly emitted but due to internal absorption, the x-ray signal is peaked into the direction of the electron beam, where the lower the energy the stronger the peak. Assuming all generated x-rays escape the sample (usually the loss of x-rays is about 5%), the information depth is related to the primary beam energy. Figure 2.8 shows the basic setup of the EDX detection system.

In the EDAX system, the detector medium is a Si(Li) crystal (a semiconductor) which converts the x-ray quantum to an electrical pulse, with a charge proportional to the energy of the detected x-ray particle. Figure 2.9 is a cross section of the detection crystal indicating the major components. The charge quantity is represented by the peak voltage and processed in an electronic setup as shown below :-

Li is incorporated into the highly pure single crystal Si to neutralise residual Boron impurities. In this totally neutral crystal where no charge carriers exist, carriers are introduced by x-rays losing their energy in Si and can be collected. In Si, it takes 3.8eV to produce a charge pot. Therefore the biasing voltage of 750V could generate a small current in the magnitude of microamperes at room temperature and mask the effect of the x-rays. Therefore the detector is cooled with liquid nitrogen to about 77^{o}K and the current is reduced to a negligible 10^{-13} amperes.

The EDX system has been widely applied to electron microscopy and has proven to be a superb qualitative and quantitative method of analysis. Among its advantages are :

- Simultaneous detection of elements
- Does not miss unexpected elements
- Rapid qualitative and comparative analysis
- Adaptable to irregular or rough samples
- Relatively compact, low power and few moving parts

2.4.4 Ultra Violet and Visible Spectroscopy (UV/VIS)

To obtain information pertaining to the absorption and transmission in the UV to Visible region of the spectrum, a UV/VIS spectrophotometer is used in analysis [56]. The UV region of a spectrum ranges from about 185 and 340nm and visible region from 340nm to 1000nm. An analysis in this region would reveal information of electronic transitions and vibrations of the fine structure. When a radiation is incident on a particular transparent sample, five different phenomena could occur namely absorption, transmission, reflection, scattering and fluorescence excitation. These incidents are shown in figure 2.10 where the interaction of light and matter is schematically indicated.

However in this case, solid transparent samples are in use and the geometry of analysis is such that the effect of scatter and fluorescence are minimal. Lambert's Law states that each layer of equal thickness of an absorbing medium absorbs an equal fraction of the radiation energy that transverses through it. Therefore the fraction of radiant energy transmitted for a thickness of absorbing medium is independent of incident radiation intensity. The various absorption phenomena are shown in figure 2.11.

If incident radiation is I_0 and transmitted radiation is I, then the fraction transmitted ,

$$\frac{I}{I_0} = T \quad \text{and percentage transmittance} \quad \%T = \frac{I \times 100}{I_0}$$

An obtained transmission fringe patterns due to atomic transitions between discrete energy bands would help deduce the refractive, absorption coefficient and film thickness through mathematical processes.

The Beer-Lambert Law states that the concentration of a substance is directly proportionate to the absorbance, A, of the particular material. This law is only true for monochromatic light and if the physical and chemical state of the substance does not change.

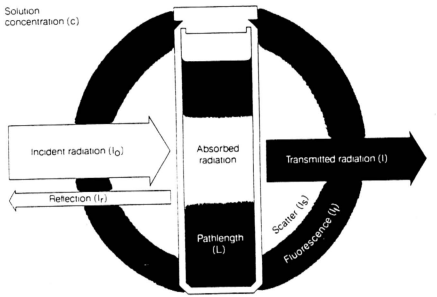

Figure 2.10 : Interaction of Light with Matter

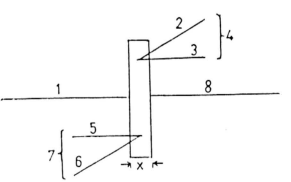

Figure 2.11 : Various Absorption Phenomena

1. Incident Radiation, I_0 (λ_0)
2. Other Photons
3. Rise in Radiation, (λ_0)
4. Total Photoelectric Effect
5. Coherent Scatter
6. Incoherent Scatter
7. Total Scatter
8. Transmitted Radiation, $I(\lambda_0) = I_0 \exp(-\mu\rho x)$

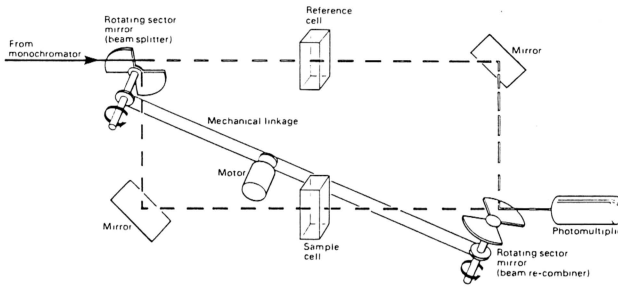

Figure 2.12 : Schematic Double Beam Optical System

Mathematically, absorbance is related to percentage transmittance by the expression :

$$A = \log \frac{I_0}{I} = \log \frac{100}{T} = KCL$$

where L = length of radiation path
C = concentration of absorbing molecules in the path
K = extinction coefficient dependent on the molecules and wavelength

The spectrophotometer used was a double beam instrument with full software controlled system with wavelength scanning abilities. The principle components of the optical system is shown figure 2.12

The UV source used for the most satisfactory operation below 340nm is the Deuterium arc lamp and tungsten quartz lamp is optimum for the radiation source in the visible to the near infrared region (340 - 1000nm). A laser etched holographic diffraction grating is used for wavelength selection and is totally software controlled, thus wavelength scanning is used with ease. The rotating beamsplitter serves to divide the intensity to two optical paths to pass through the reference and sample position and a beam recombiner brings together these two signals and focuses it into a photo multiplier tube. Signal processing, manipulation and storage is done via a computer.

2.5 Electrical Characterisation

Cadmium Tellurite (CdTe) and Cadmium Selenide (CdSe) are frequently used materials as solar absorbers [57-63]. The ability of n-CdTe and n-CdSe thin films to form a heterojunction with the p-type silicon substrate naturally forms a photovoltaic cell. This is of course, a source of interest as one of the goals of this research is to investigate if the ternary compound, $CdTe_xSe_{1-x}$, derived from CdTe and CdSe, would have a favourable improvement in its solar properties.

One of the fundamental ways of gauging the solar properties is by measuring the open circuit voltage and investigating the internal resistance of the fabricated solar cell. Consequently, the short circuit current (Isc) can also be derived.

2.5.1 Open Circuit Voltage, Internal Resistance (R_i) and the Short Circuit Current (I_{sc}) of the Cadmium Based Films

The open circuit voltage value is defined as the voltage across an infinite load resistance. This simply means that the voltage across the device is measured with no external load but only the consequent internal load which is the resistance of the cell and its electrical contact interfaces. In the trial stages when a variety of parameters were varied in the electrodeposition, the OCV measurement provided a brief performance profile to gauge if the change in parameters had a positive effect of the cell performance.

The apparatus setup for the measurement is shown schematically in Figure 2.13. In terms of preparation of this sample for measurement, the following steps were taken and consistently maintained for all further analysis to make an accurate comparison between measurements. The source of illumination was a 200W tungsten filament lamp, which was kept at a constant distance of 25cm from the photovoltaic cell. A closer distance would cause the sample to be heated up and lose whatever gain due to increased intensity. A fixed area of 1.5 x 1.5cm was illuminated and the rest of the surface area was masked with an insulating sheet. A thin streak of silver paint was applied on the deposited film with a length of about 1cm to function as a current collector for the front face electrode. The schematic assembly as shown in Figure 2.13 is constructed with a digital multimeter used in the >500mV range, as the voltmeter. Connections were made from the multimeter to the silver paint contact and the silicon substrate. Upon perpendicular illumination by the tungsten lamp, the photovoltage is measured by the voltmeter and is recorded as the OCV.

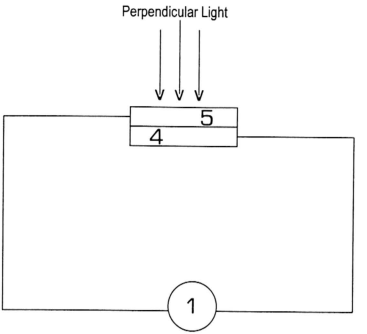

Figure 2.13 : Apparatus Steup for the OCV Measurement

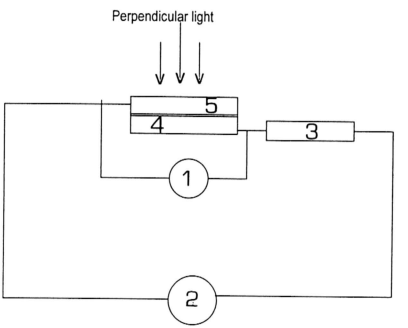

Figure 2.14 : Apparatus Setup for Current - Voltage Measurement

Key:
1. Voltmeter
2. Microammeter
3. Resistance Box
4. Silicon Substrate
5. Cadmium Based Film

To measure the internal resistance of the cell, the multimeter was switched to the resitance measurement range (<20 MΩ) and the resistance is measured also under the illumination of the lamp. It was found to be impractical to measure the short circuit current in the same way as the current obtained is in the region of μA and very prone to fluctuations. Therefore from the relationship V = IR, we can compute the current value I_{sc} which is the short circuit current.

2.5.2 The Current-Voltage Characteristic Curve

A photovoltaic (PV) cell can be represented by a circuit with a constant current generator with an ideal diode across it to simulate a p-n junction as discussed in section 1.10. The apparatus used for generating the current-voltage (I-V) values is shown schematically in Figure 2.14. The PV cell is placed in series with a resistance bridge and a Kiethley benchtop multimeter set in the μA measurement range. A digital multimeter was set in the >500mV range and placed parellally across the PV cell. With the higher load placed in series with the PV cell, the amount of current drawn now becomes higher and it becomes realistic to actually measure the current in the circuit, unlike in section 2.3.1. By varying the resistance, the changes in the voltage and current were noted down and plotted against each other to form the I-V characteristic curve.

By comparing the shape of the I-V curve with ideal values, it allows us to deduce the internal characteristics which are described as the series resistance and shunt resistance. The effects of these phenomenons are described in section 1.10 and the respective I-V curves. The series resistance of a PV cell arises from the sheet resistance, the metal semiconductor contacts and the substrate resistance. The shunt resistance effect arises from leakage paths around the junction area. The most significant information that can be deduced from the I-V curve is the total amount of power that can be generated from a solar cell. By merely comparatively viewing the curves, a general comparison can be made on the efficiency, providing all other parameters are kept constant. This information can be studied in greater detail by calculating the fill factor and efficiency (described in chapter 1) from the curve.